

**Nature and strength of defect interactions in cubic stabilized zirconia**

A. Bogicevic and C. Wolverton

*Scientific Research Laboratories, Ford Motor Company, Dearborn, Michigan 48124*

(Received 12 July 2002; published 17 January 2003)

The intrinsic ordering tendencies that limit ionic conduction in doped zirconia electrolytes are fully elucidated using first-principles calculations. A detailed analysis of nearly 300 yttria- and scandia-stabilized cubic-zirconia-ordered vacancy compounds reveals a delicate balance between competing elastic and electrostatic interactions. These results explain several outstanding experimental observations and provide substantial insight needed for improving ionic conduction and enabling low-temperature operation of zirconia-based electrolytes. We show that the surprising  $\langle 111 \rangle$  vacancy ordering in dilute solid solutions is a consequence of repulsive electrostatic and attractive elastic interactions that balance at third-neighbor vacancy separations. In contrast, repulsive elastic vacancy-dopant interactions prevail over electrostatic attraction at all probed defect separations in YSZ and lead to very weak ordering preferences in ScSZ. The total electronic contribution to the defect interactions is shown to be strongly dominated by simple point-charge electrostatics, leaving speculation of defect ordering for a given class of aliovalent dopants to the elastic term. Thus, ion size becomes a critical parameter in controlling the ionic conductivity of doped oxide electrolytes.

DOI: 10.1103/PhysRevB.67.024106

PACS number(s): 64.60.Cn, 81.30.Dz, 61.18.-j, 71.15.Mb

**I. INTRODUCTION**

Zirconia-based ceramics are found in a remarkable variety of technological and commercial applications, e.g., thermal barrier coatings, gas sensors, catalyst washcoats, solid oxide fuel cells, and even fashion jewelry. This impressive versatility originates from the creation of atomic defects in the zirconia crystal. As certain aliovalent (nonisovalent) oxides are added to  $\text{ZrO}_2$ , substitutional cations are charge balanced by the formation of anion vacancies. These defects and their mutual interactions dramatically affect the structural, thermal, mechanical, and electrical properties of zirconia. Perhaps the most conspicuous example comes from the many orders of magnitude increase in the ionic conductivity of zirconia upon aliovalent doping, facilitated by the diffusion of oxygen vacancies.<sup>1,2</sup>

Because ionic transport in this class of materials is tied directly to atomic defects, it automatically follows that any interactions among these are prone to affect the ionic conductivity. The severity of defect interactions is best illustrated by the exponential decay in ionic conductivity beyond some critical oxide composition, despite an increasing number of charge carrying vacancies. Defect interactions are thus believed to be the primary source of two highly unwelcome limitations of zirconia-based (and other) electrolytes: (i) a sharp drop-off in ionic conductivity beyond a relatively low level of aliovalent doping (typically 8–12 mol %) and (ii) a remarkable sensitivity of the ionic conductivity to the thermal history of the electrolyte and accompanying fluctuations in oxide composition.<sup>1–3</sup>

Despite these overwhelming effects on ionic conduction and other microscopic properties of zirconia ceramics (and related materials classes), there is currently no  $\text{ZrO}_2$ -based oxide system where the origin and strength of defect interactions are completely known. Weak scattering contrast and other experimental difficulties together with the computational demands of sufficiently accurate theoretical modeling have both contributed to this situation.<sup>4,5</sup> For example, even

for the most well-utilized and well-studied zirconia ceramic, yttria-stabilized zirconia (YSZ), there is an abundance of contradictory experimental reports of whether oxygen vacancies prefer to bind to dopant ( $\text{Y}^{3+}$ ) (Refs. 6–11) or host ( $\text{Zr}^{4+}$ ) (Refs. 12–16) cations. Existing physical models have proved of limited value, insofar as often being in mutual disagreement, remaining unverified and failing to explain variations due to the chemical identity of the dopant.<sup>4,5</sup>

First-principles studies have recently proved helpful in unraveling some of these complex defect interactions.<sup>4,5,17–19</sup> By analyzing the energetic preferences of various ordered doped zirconia compounds, the intrinsic defect ordering tendencies can be established. In previous studies, we found that there are opposing forces at play for vacancy-dopant interactions<sup>5</sup> and that dopant size has a strong effect on defect ordering.<sup>4</sup> Still, several important issues like vacancy-vacancy and dopant-dopant ordering remain poorly understood. An important goal of this study is to establish these defect ordering preferences and relate them to ionic conductivity.

Knowing *how* defects interact in stabilized zirconia is instrumental to understanding its ionic conductivity and other materials properties. In the following, we therefore examine these interactions in detail. In addition, we are concerned with the generality of these results, i.e., how well they transfer to other doped zirconia compounds and even other oxide electrolytes. As we will show, there are both great similarities and striking differences between yttria- and scandia-stabilized zirconia (ScSZ) alone. Knowing *why* defects interact the way they do provides insight that can be used to assess such questions of transferability and even help guide rational design. Thus, the principal focus of this paper is to identify the origin of the computed defect ordering tendencies.

In this paper, we present a first-principles study of the nature and strength of defect interactions in yttria- and scandia-stabilized zirconia. A detailed analysis of a large number of ordered vacancy compounds, coupled with strate-

gic interaction decompositions and separate electrostatics calculations, provides several important new results regarding the defect chemistry in doped zirconia.

(i) The nature *and* magnitude of intrinsic vacancy-vacancy, vacancy-dopant, and dopant-dopant interactions are all thoroughly elucidated and related to the observed short-range order in solid solutions and long-range order in compounds. The magnitude of the interactions decays as vacancy-vacancy > vacancy-dopant >> dopant-dopant.

(ii) Defect ordering preferences are without exception shown to arise from a competition between electrostatic (dopant independent) and elastic (highly dopant dependent) defect interactions.<sup>20</sup> The best way to minimize vacancy-dopant association deleterious to ionic conduction is to choose dopants which induce a finite strain that counteracts the electrostatically driven ordering, i.e., not to strive for zero strain.

(iii) It is safe to use the term electrostatics because we prove that the complex quantum-mechanical electronic interactions are comprised predominantly of simple classical point-charge electrostatic Coulomb interactions when elastic interactions are treated separately.

(iv) The experimentally observed vacancy ordering in dilute solutions as well as ordered compounds is explained in terms of a balance between competing vacancy interactions.

(v) The complete crystal structures of experimentally observed ordered compounds are established (e.g., the  $\delta$  and  $\gamma$  phases of ScSZ) and shown to be fully consistent with deduced defect ordering tendencies. This includes the non-trivial result that the two ordered  $\delta$  phases of YSZ and ScSZ differ in crystal structure due to variations in the elastic term of vacancy-dopant interactions.

(vi) Variations in ionic conduction due to dopant species are traced back primarily to ion size-induced differences in the elastic part of vacancy-dopant interactions.

(vii) Said results are proved valid for a wide range of dopant concentrations (at least within 14–40 mol %).

The paper is organized as follows: Section II describes our theoretical approach, while Sec. III is devoted to the crystal structure and types of defect interactions on the fluorite lattice. In Sec. IV, we present our results for the nature and strength of vacancy-vacancy, vacancy-dopant, and dopant-dopant interactions, and in Sec. V we report on point-charge electrostatics calculations. In Sec. VI we discuss long-range order and the predictions of new ordered YSZ and ScSZ compounds, while Sec. VII formulates our conclusions. Finally, the Appendix contains some salient technical results.

## II. THEORETICAL APPROACH

Our electronic-structure calculations are based on density-functional theory (DFT),<sup>21,22</sup> with core-valence electron interactions represented by ultrasoft Vanderbilt pseudopotentials,<sup>23</sup> as implemented in the highly efficient VASP code.<sup>24</sup> We expand the one-electron wave functions in a plane-wave basis with an energy cutoff of 29 Ry, keeping semicore electrons in the valence for all cations. For the exchange-correlation functional, we use the PW91 imple-

mentation of the generalized gradient approximation (GGA).<sup>25</sup> Technical details about the use of the local density approximation (LDA)<sup>26</sup> and pseudopotential variations are described in Ref. 4. We solve the Kohn-Sham equations iteratively and optimize all atomic positions, cell shape, and cell volume using a conjugate gradient algorithm until residual atomic forces are less than 0.03 eV/Å. The Brillouin zone sampling<sup>24</sup> is performed using increasingly more dense Monkhorst-Pack  $\mathbf{k}$ -point meshes, until absolute convergence is achieved (to  $\leq 1$  meV/unit cell). In most cases, a  $(4 \times 4 \times 4)$   $\mathbf{k}$ -point mesh is sufficient and forms the basis for all results except the large cell  $Zr_{10}M_4O_{26}$  calculations where a  $(2 \times 2 \times 2)$   $\mathbf{k}$ -point mesh is used. To enhance convergence with respect to Brillouin zone sampling, we employ a Fermi smearing of the electronic occupancy with a fictitious electronic temperature of 0.2 eV and then extrapolate to zero temperature. In certain structures where the band gap turns out to be substantially decreased, a smaller smearing width of 0.1 eV is used to reduce the electronic entropy below 1 meV/ion. All calculations employ primitive unit cells, which entail 11–40 atoms per cell.

## III. FLUORITE LATTICE

Pure zirconia crystallizes in three different structures, depending on the temperature. For a discussion of the monoclinic and tetragonal polymorphs of  $ZrO_2$ , we refer the reader to Ref. 4 and references therein. The cubic fluorite phase is thermodynamically stable only above about 2650 K.<sup>16</sup> The substitution of lower-valent cations for tetravalent Zr ions results in the creation of charge compensating anion vacancies. For trivalent dopants like Y and Sc, one oxygen ion is removed for every two dopant cations introduced into the zirconia lattice. The most pronounced crystallographic effect upon aliovalent doping is the effective stabilization of the tetragonal and cubic phases towards lower temperatures. The easy transport of oxygen ions via anion vacancy diffusion in these phases is directly responsible for the considerable increase in ionic conductivity upon aliovalent doping.

The stabilized cubic phase of  $ZrO_2$  poses an interesting, multifaceted ordering problem. The fluorite structure consists of two sublattices: an fcc sublattice, hosting Zr and dopant cations, and a simple cubic sublattice, hosting oxygen ions and oxygen vacancies (denoted  $\square$ ). This dual sublattice geometry leads to three distinct forms of intrasublattice and intersublattice interactions (see Fig. 1):

(1) cation/cation interactions on the cation sublattice

$$(Zr/Zr, M/Zr, M/M),$$

(2) anion/anion interactions on the anion sublattice

$$(O/O, \square/O, \square/\square),$$

(3) cation/anion interactions between the sublattices

$$(Zr/O, M/O, Zr/\square, M/\square),$$

where  $M$  denotes the aliovalent cation dopant (Y or Sc here). Each of these three interactions may be either of “ordering type” (association of unlike species, e.g., Y and  $\square$ ) or “clus-

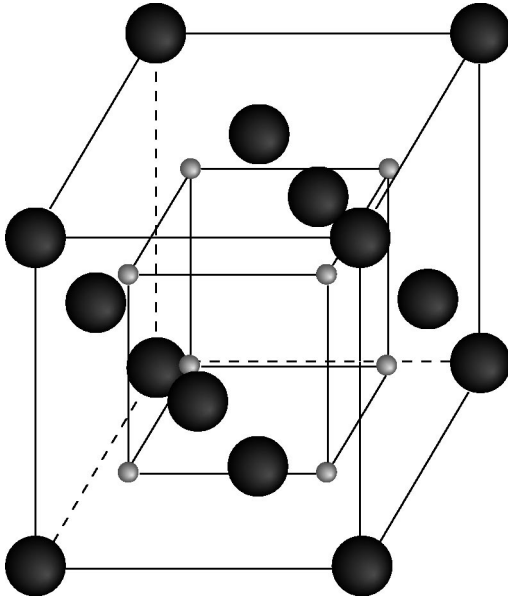
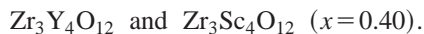
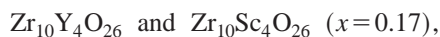
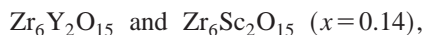


FIG. 1. Schematic illustration of the fluorite lattice, showing how it can be viewed as coupled fcc cation and simple cubic (sc) anion sublattices. The anions are small for clarity (though they are actually larger than the cations). In the case of cubic-stabilized zirconia, the fcc sublattice hosts  $Zr^{4+}$  and dopant (e.g.,  $Y^{3+}$  or  $Sc^{3+}$ ) cations, while the sc sublattice hosts  $O^{2-}$  ions and their vacancies.

tering type” (association of like species) and depends on the separation shell, i.e., nearest neighbor, next nearest neighbor, etc.). In addition, these three interactions, and thereby also the ordering tendencies, tend to be highly coupled, underscoring the complexity inherent in this seemingly simple system. Although it makes good sense to initially focus on pair interactions, a complete description must in principle also take into account many-body interactions.

In this study, we investigate the origin and strength of defect ordering tendencies in stabilized zirconia (SZ) via the energetic dependence of the total cation and anion configuration, as calculated from first principles. The complete ranges of compositions studied (with the mole fractions of yttria/scandia,  $x$ ) are



Once the cation configurations are specified, all possible symmetrically distinct anion ordering possibilities are enumerated using advanced lattice algebra techniques developed for Ising-model studies of alloys.<sup>27</sup> The full details of this procedure are described in a previous study,<sup>4</sup> which also reports some of our early YSZ results. The defect ordering preferences are measured by energetic preferences. By combining  $ZrO_2$  and  $M_2O_3$  ( $M=Y$  or  $Sc$  here) with mole frac-

tions  $1-x$  and  $x$ , respectively, one obtains an *MSZ* stoichiometry given by  $Zr_{1-x}M_{2x}O_{2+x}$ . The formation enthalpy of this *MSZ* compound is then given by the (zero-pressure) energy difference between the *MSZ* compound and the composition-weighted average of its constituent oxides (cubic  $ZrO_2$  and bixbyite<sup>28</sup>  $M_2O_3$ ):

$$\Delta H = E[Zr_{1-x}M_{2x}O_{2+x}] - [(1-x)E(ZrO_2) + xE(M_2O_3)].$$

A negative formation enthalpy indicates the stability at 0 K of the compound relative to phase separation into the constituent oxides, whereas a positive formation enthalpy indicates that phase separation is preferred in the absence of entropic effects at finite temperatures. Although our calculations are for zero temperature (i.e., no entropic effects are included), they allow us to uncover the generic ordering tendencies that exist in these systems.

Figures 2 and 3 show the DFT-GGA-computed formation enthalpies for an ensemble of YSZ and ScSZ compounds at five different dopant concentrations. A discussion about the relative energies of these compounds and their implications for long-range order is presented in Sec. V. A few things can be noted immediately though. First of all, it is clear from Figs. 2 and 3 that within any given stoichiometry, there is a large scatter in formation enthalpies depending on the detailed cation+anion configuration. The span of this scatter gives a first indication of the energetic magnitude of the combined defect ordering. Second, in several cases, the formation enthalpy span crosses the  $\Delta H=0$  line, indicating that the detailed ordering can qualitatively determine whether or not formation is energetically preferable. Finally, there are obvious similarities as well as qualitative differences between the energies of YSZ and ScSZ which are not *a priori* understood. We explain these differences below.

#### IV. DEFECT INTERACTIONS

To better assess the questions of how defects interact in zirconia and what causes them to do so, we separate the defect interactions into elastic and electronic contributions. We perform this separation by evaluating all SZ structures in two different manners, with two distinctly different energy scales. In the first case, the atoms are kept in their ideal fluorite positions by freezing out ionic relaxations, and the defects are thus prohibited from interacting elastically. To make energetic evaluations meaningful, all ordered compounds within any given crystal structure and composition are made using the same volume and cell shape. The computed formation energies of these restrained cells are therefore always positive and quite large.<sup>29</sup> The absolute values reflect the large energetic gain to be had upon ionic relaxations (the energies associated with cell-external optimization, i.e., cell shape and cell volume, are quite small compared with cell-internal relaxations). This procedure lets us assess the defect ordering tendencies with only electronic interactions between the ions in the crystal, as determined by comparing the relative energies of unrelaxed isomorphic structures. In the second case, we allow full ionic relaxations while optimizing cell shape and volume, as described in Sec. II. This lets us evaluate defect interactions as a result of both

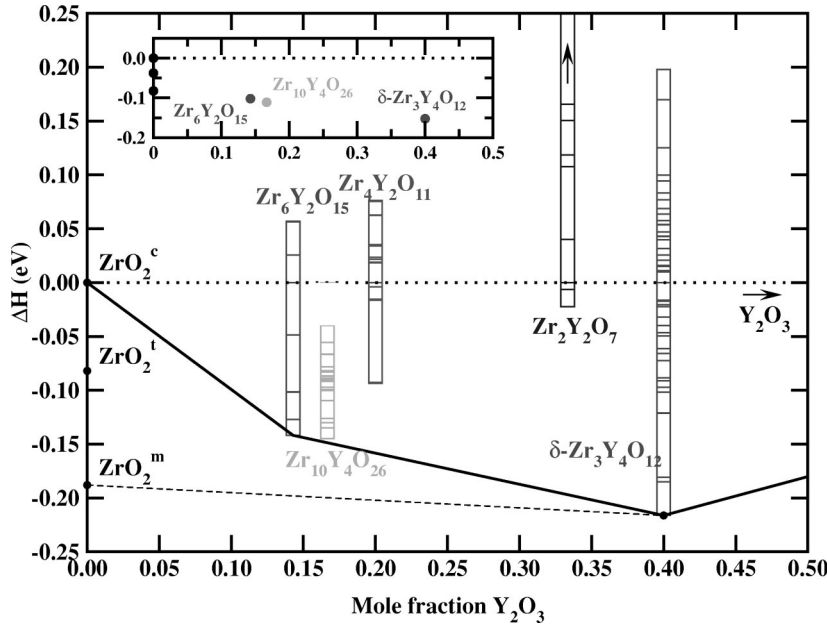


FIG. 2. Formation enthalpies (eV per  $Zr_{1-x}Y_{2x}O_{2+x}$  formula unit) and convex hull construction for a number of YSZ compounds at five different compositions (see Sec. VI for a discussion about convex hulls). The inset illustrates LDA results for the GGA hull structures. Solid lines represent the convex hull connecting low-energy structures based on the cubic fluorite lattice (i.e., excluding the tetragonal and monoclinic  $ZrO_2$  phases). The dashed line represents the convex hull including all phases considered.

electronic and elastic interactions. The energetic difference between the two cases defines the elastic part of the total defect ordering tendencies. A further decomposition of the electronic contribution to the defect interactions into electrostatic and other components is presented in Sec. V.

In the following, we report analyses of the nature and strength of vacancy-vacancy, vacancy-dopant, and dopant-dopant interactions in three separate subsections and then perform a decomposition of the electronic interactions.

**A. Vacancy-vacancy interactions**

Based on simple point charge electrostatics, vacancies are expected to repel one other because of the +2 lattice-relative charge they carry with them. The six closest neighbor shells for the simple cubic (sc) anion lattice in the fluorite structure and their respective separation are

- (1)  $\langle 100 \rangle (a)$ ,
- (2)  $\langle 110 \rangle (\sqrt{2}a)$ ,
- (3)  $\langle 111 \rangle (\sqrt{3}a)$ ,
- (4)  $\langle 200 \rangle (2a)$ ,
- (5)  $\langle 210 \rangle (\sqrt{5}a)$ ,
- (6)  $\langle 211 \rangle (\sqrt{6}a)$ ,

where  $a$  is the nearest-neighbor oxygen vacancy separation, which is around 2.7 Å in YSZ compounds and about 2.5 Å in ScSZ compounds.

A number of diffuse neutron and x-ray scattering experiments of YSZ have shown a strong tendency for anion vacancies to align along  $\langle 111 \rangle$ , i.e., as third neighbors, in both the ordered  $\delta\text{-Zr}_3\text{Y}_4\text{O}_{12}$  compound and the solid solution fluorite phase of YSZ.<sup>16,30–32</sup> The first observation makes perfect sense from an electrostatic point of view, because the  $\langle 111 \rangle$  direction represents the largest average separation va-

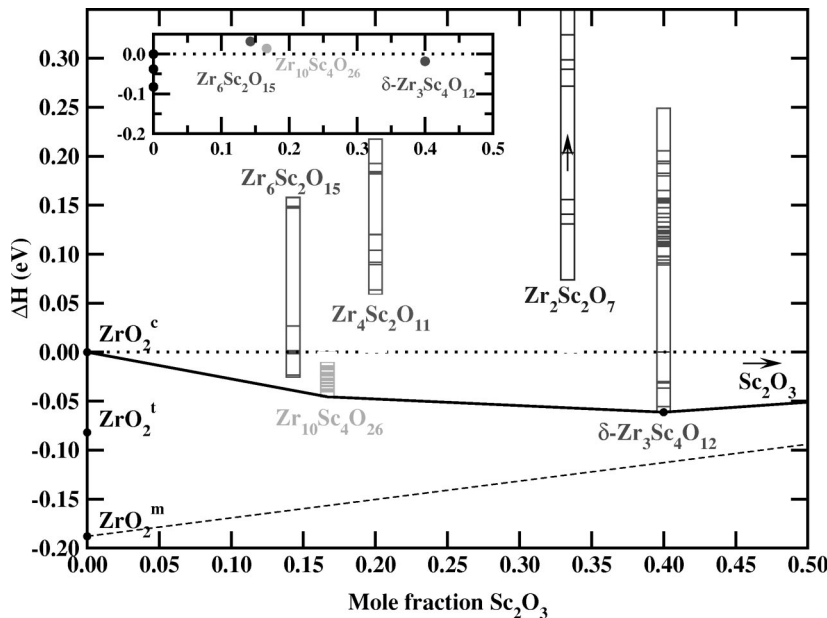


FIG. 3. Formation enthalpies (eV per  $Zr_{1-x}Sc_{2x}O_{2+x}$  formula unit) and convex hull construction for a number of ScSZ compounds at five different compositions. Solid lines represent the convex hull connecting low-energy structures based on the cubic fluorite lattice, while the dashed line represents the convex hull including all phases considered. The inset illustrates LDA energies for the GGA-preferred hull structures (cf. Fig. 2).

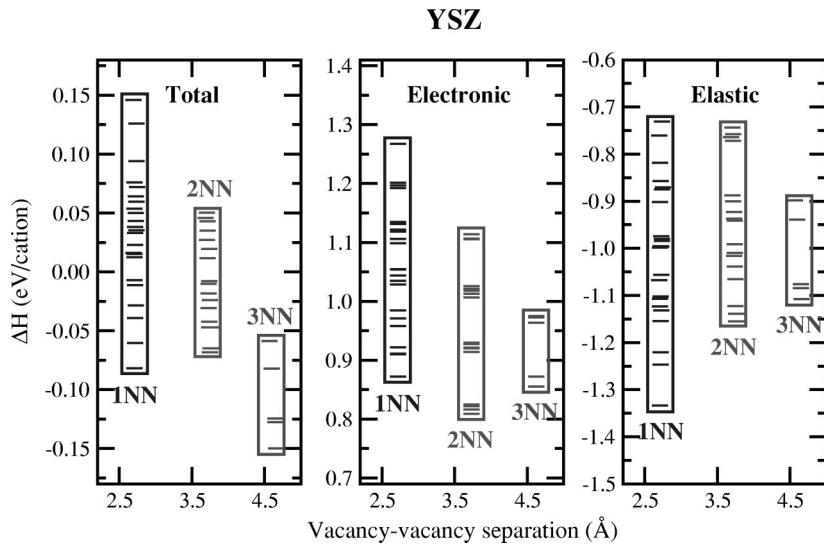


FIG. 4. Calculated formation enthalpies (eV/cation) vs vacancy-vacancy separation for 45 different  $Zr_3Y_4O_{12}$  compounds. The total formation enthalpies (left) are decomposed into electronic (middle) and elastic (right) contributions, as discussed in the text. The data are categorized by the three possible vacancy-vacancy shells (1NN, 2NN, 3NN).

cancies can achieve at 40 mol % doping. Vacancy alignment along  $\langle 111 \rangle$  in dilute solid solutions, however, is quite unexpected because there is nothing obvious hindering the vacancies from assuming larger separations than third neighbors, which is what one would expect on purely electrostatic grounds. Since vacancy clustering is believed to be a major, if not the principal, limiting factor of ionic conductivity in this class of oxide conductors,<sup>1-3</sup> there is an obvious interest in understanding this vacancy behavior.

Out of the five different compositions considered here, the 40 mol % and 17 mol % compounds offer the best opportunity to address vacancy-vacancy interactions since there are two vacancies per unit cell of  $Zr_3Y_4O_{12}$  and  $Zr_{10}Y_4O_{26}$ . For the unrelaxed fluorite lattice, the vacancy positions are well defined. For the relaxed cells, we simply take these ideal fluorite cell-internal positions as the vacancy coordinates.

### 1. 40 mol % composition

We begin our analysis of vacancy ordering tendencies with the 40 mol % so-called  $\delta$  compounds of YSZ and ScSZ (described in detail in Sec. VI). Figures 4 and 5 show the

computed formation enthalpies versus vacancy-vacancy separation for the 45  $Zr_3Y_4O_{12}$  and 45  $Zr_3Sc_4O_{12}$  structures. Focusing on the leftmost panels of Figs. 4 and 5, we immediately draw several conclusions: Large (third neighboring) vacancy-vacancy separations seem to be energetically preferred for both YSZ and ScSZ, and the substantial vertical spread within each vacancy-vacancy shell (which obscures this observation) is indicative of the combined strength of vacancy-dopant and dopant-dopant interactions.

In the remainder of Figs. 4 and 5, these vacancy-vacancy interactions are decomposed into electronic and elastic contributions, as explained above. The fact that third-neighboring (3NN) vacancy structures on average are the most favored ones when relaxations are frozen (middle panels) shows that the vacancy-vacancy repulsion is electronic in origin. In contrast, a look at the rightmost panels in Figs. 4 and 5 shows that the elastic part of the interactions appears to prefer a close vacancy-vacancy association, apparently counteracting this repulsion. This contrast is the first indication that there are opposing forces at play, at least when it comes to vacancy-vacancy ordering in stabilized zirconia.

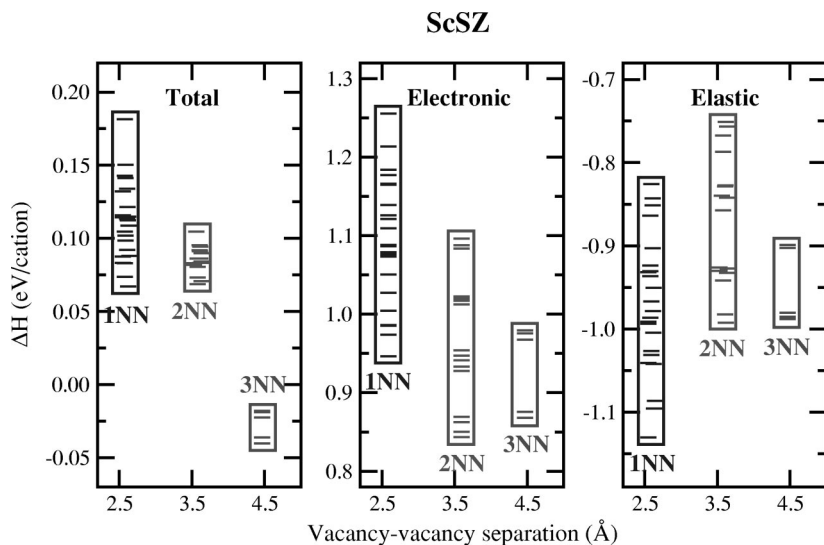


FIG. 5. Same as Fig. 4 for  $Zr_3Sc_4O_{12}$ .

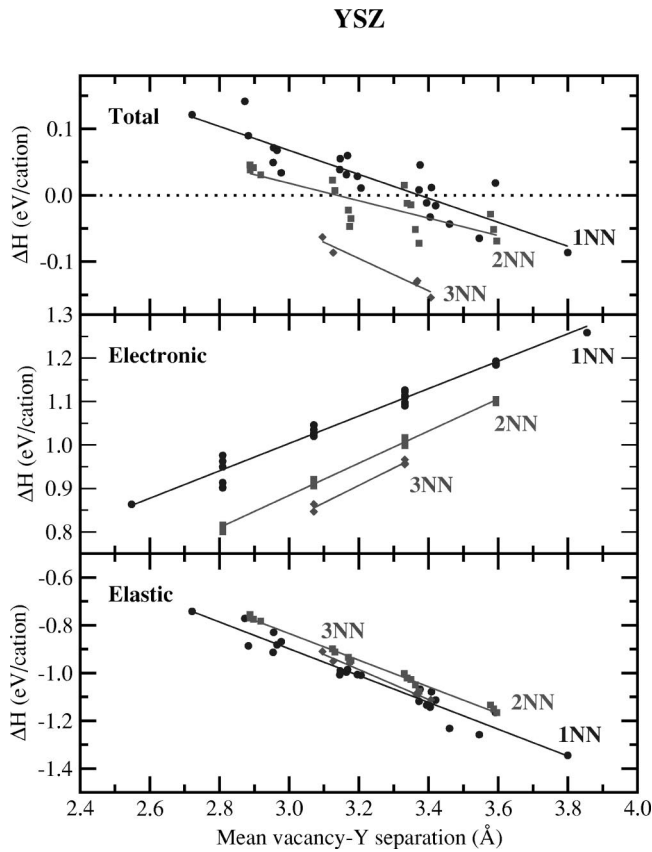


FIG. 6. Calculated formation enthalpies (eV/cation) vs mean vacancy-dopant separation for 45 distinct  $Zr_3Y_4O_{12}$  compounds. The total formation enthalpies are decomposed into electronic and elastic contributions, as in previous figures. The circles, squares, and diamonds represent 1NN, 2NN, and 3NN vacancy-vacancy configurations, respectively. The lines represent linear regressions of the data sets and are primarily there as a guide to the eye. The relative vertical order of these lines indicate vacancy-vacancy ordering preferences, while the slopes reflect the preferred vacancy-dopant ordering.

Although Figs. 4 and 5 do give us a first indication of the origin and strength of the vacancy-vacancy interactions, the picture becomes considerably clearer when we redraw the same information in a way that helps separate out the other defect ordering contributions to the scatter in the data. Figures 6 and 7 show the same data as do Figs. 4 and 5, but this time with the mean vacancy-dopant separation on the horizontal axis. These figures let us compare the energies of different vacancy-vacancy shell configurations with similar average vacancy-dopant interactions, significantly clarifying the interactions trends. In analyzing Figs. 6 and 7, we for the time being concentrate only on the vertical order of the different vacancy-vacancy shells. (The slopes of the data are of course connected to vacancy-dopant interactions, which is an interesting topic discussed in the next subsection.) The top panels of these two figures show that at any given mean vacancy-dopant concentration, third neighboring vacancies are clearly preferred over second- and first-neighbor vacancy pairs. Thus, in both  $\delta$  compounds of YSZ and ScSZ, it is now perfectly clear that vacancies do indeed repel each other

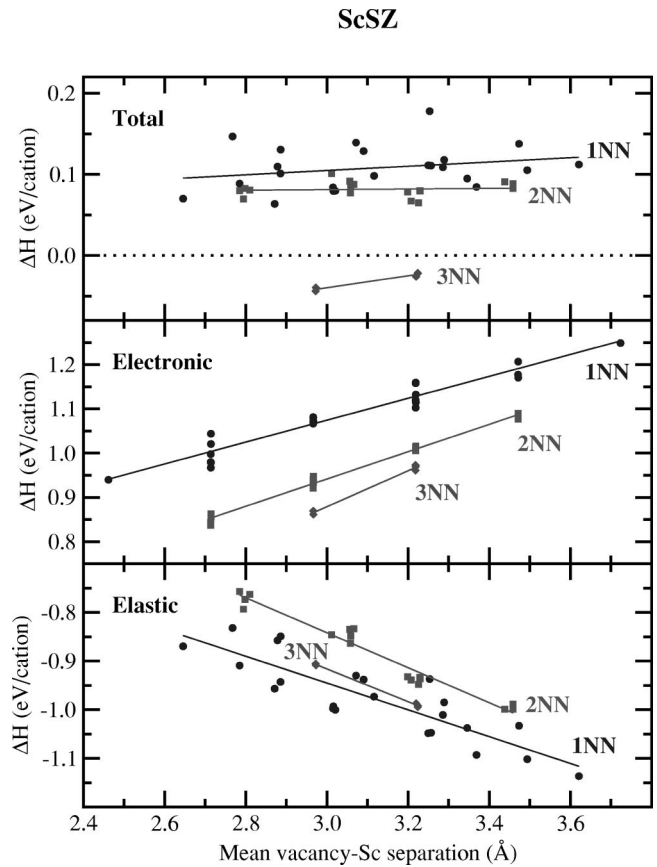


FIG. 7. Same as Fig. 6 for  $Zr_3Sc_4O_{12}$ .

and prefer to space themselves along  $\langle 111 \rangle$ . An indication of the strength of the vacancy-vacancy repulsion is given by the energy scale on the ordinate.

The remainder of Figs. 6 and 7 is devoted to the decomposition of vacancy interactions into electronic and elastic contributions. These analyses clearly show that the vacancy-vacancy repulsion is electronic in origin: at any given mean vacancy-dopant separation, all 3NN vacancy structures are favored over 2NN configurations, which in turn are favored over NN vacancy structures in the absence of elastic interactions. It is also evident from the bottommost panels that the elastic part of the vacancy interactions counteracts the electronic repulsion, but that the elastic attraction at these vacancy separations is too weak in both YSZ and ScSZ to overturn the strong electronic repulsion. Hence, the repulsive vacancy-vacancy character dominates the total vacancy interaction at these compositions (vacancy separations).

### 2. 17 mol % composition

At this point, one might wonder how these ordering tendencies translate to lesser dopant concentrations, commonly used in practical zirconia applications. In addition, we still have not addressed the unexpected  $\langle 111 \rangle$  3NN vacancy ordering observed experimentally in dilutely doped zirconia. To address both these questions, we now shift our focus to the 17 mol % compounds  $Zr_{10}Y_4O_{26}$  and  $Zr_{10}Sc_4O_{26}$ . The analyses for these compounds are perfectly analogous to the ones described so far, except that in this case the larger unit

cells let us probe vacancy-vacancy interactions out to 6NN vacancy shells (the maximal separation taking into account cell replica interactions). Thus, we are prepared to address the important questions of whether the 3NN vacancy-vacancy ordering observed at higher dopant concentrations persists at more dilute doping, as suggested in numerous experiments, and how this can be understood.

The  $Zr_{10}M_4O_{26}$  structure is actually most well suited for analyzing cation-cation ordering tendencies, and the relevant lattice algebra analysis of this structure is deferred to Sec. IV C. For the present purposes, we note that there is a grand total of 48 ordered structures with 3NN vacancies in  $Zr_{10}Y_4O_{26}$  and  $Zr_{10}Sc_4O_{26}$ , for which the energies are reported in detail in Sec. IV B. We now compare these ordered structures with cases where we put the vacancies as far apart as possible (6NN along  $\langle 211 \rangle$ ).

We find that all of the 48 Y-doped and Sc-doped structures (each with 3NN vacancies) have a negative formation enthalpy (see Figs. 2 and 3), indicating an energetic “reward” for 3NN vacancy ordering. As we separate these vacancies further, to 6NN, we achieve the two least favorable formation enthalpies in the entire ensemble. Thus, in excellent agreement with experimental findings,<sup>16,30–32</sup> we too find that 3NN vacancy ordering is preferred over larger vacancy separations (with the limited 6NN data we have). While this is reassuring for our theoretical methodology, it still begs an explanation, since it seemingly defies a simple electrostatic argument.

To shed some light on this outstanding question, we again turn to our method of decomposing the defect interactions into elastic and electronic components. Remarkably, we find that when elastic interactions are frozen the very same 6NN structures become the two most favored ones, out of 50 distinct  $Zr_{10}M_4O_{26}$  structures. Thus, there cannot be any doubt that the electrostatically expected defect ordering (6NN preferred over 3NN) is indeed realized when elastic interactions are absent and that it is the elastic component that counteracts the electronic interactions. This balance between electrostatic repulsion and elastic attraction between vacancies leads to an energetic minimum at a 3NN vacancy separation, explaining the experimental observations at dilute doping. We note that this argument is valid both for YSZ and ScSZ, although the 3NN well is somewhat more shallow in the case of ScSZ due to its weaker elastic component.

## B. Vacancy-dopant interactions

In this section, we next consider the interaction of the dopant cations with their charge compensating anion vacancies. It is easy to see how a strong anion-cation ordering tendency could inhibit ionic conduction by tying up vacancies and slowing their diffusion, so this ordering merits some close consideration. Experimentally, the most studied zirconia conductor is YSZ. As mentioned previously, experimental data for vacancy-dopant ordering in YSZ have been inconclusive, although the most recent data seem to indicate that vacancies prefer to bind to host (Zr) over dopant cations.<sup>16,12,15</sup> Theoretical first-principles calculations by Stapper *et al.*<sup>18</sup> and ourselves,<sup>4</sup> as well as semiempirical cal-

culations by Sakib Khan *et al.*<sup>33</sup> and Zacate *et al.*,<sup>34</sup> all corroborate these recent experimental findings. Yet based on electrostatics, one would expect just the opposite: namely, a vacancy-dopant attraction due to the relative point charges of  $1-$  and  $2+$  for dopant and vacancies. Theoretical models based on cation coordination rationalize the vacancy-Zr association in YSZ from the preferred tendency for Zr ions to assume sevenfold coordination, as in the monoclinic ground state (zero-pressure equilibrium phase) of  $ZrO_2$ . However, this reasoning fails to account for dopant species variations (as do purely electrostatic models) and is contradicted by the preferred sixfold coordination of Zr in the ordered  $\delta$  compound of YSZ (see below).<sup>4</sup> A more detailed account of the experimental and theoretical background is given in Ref. 4.

The main results of our vacancy-dopant interaction studies are contained in Figs. 6 and 7, which contain energies for the 40 mol % yttria and scandia compounds. While in the previous section we were concerned with the vertical energetic order of the vacancy subshells, the appropriate measure in this case is the slope of the  $\Delta H$  versus mean vacancy-dopant separation. For the computation of the latter quantity, we again use ideal vacancy positions and then take an average of all separations between vacancies and nearest-neighbor dopant ions.

We first focus on the YSZ results of Fig. 6. The negative slope within each of the three vacancy-vacancy subshells in the top panel demonstrates a clear preference for vacancy-Zr association, as reported previously.<sup>4</sup> To understand this result, we decompose the interaction energies into electronic and elastic components in the remaining two panels of Fig. 6. The positive slopes in the middle panel clearly show that in the absence of strain interactions, vacancies indeed do prefer to bind to  $Y^{3+}$  ions, as expected from electrostatic considerations. The negative slopes in the elastic part of the interaction (bottommost panel) distinctly show that the electrostatic ordering tendencies are counteracted by the elastic term. Thus, just like in the case of vacancy-vacancy ordering, we have a balance between two opposing forces controlling defect ordering in YSZ. However, there are two important distinctions to keep in mind. First of all, the signs of the elastic and electronic interactions are reversed; the elastic component is attractive (repulsive) for vacancy-vacancy (vacancy-dopant) ordering, with the electronic part in both cases counteracting the elastic term. Second, this balance is reached at 3NN for vacancy-vacancy ordering, while the elastic term dominates vacancy-dopant ordering at all separations probed in this study.

We now repeat this analysis for ScSZ. While the bottom two panels in Fig. 7 exhibit qualitatively similar results as the YSZ results in Fig. 6, the top panel looks markedly different. The reason for this is quite simple. A look at the bottom panel of Fig. 7 reveals that although the elastic component of the vacancy-dopant interaction is repulsive in ScSZ, just like in YSZ, it is about half as strong. This is a consequence of the considerably smaller size mismatch between  $Sc^{3+}$  and  $Zr^{4+}$ , compared with the  $Y^{3+}-Zr^{4+}$  mismatch (the Zr and Sc ions have an ionic radius of about 0.80 Å; the Y ion radius is about 0.93 Å). The net result of adding up the electronic and elastic interactions is that there is no

clear preference for the vacancies to bind to either of the two cations (near zero slope in the graph). This is the crux of the recipe for a good ionic conductor: minimize the preference for the vacancies to get bound to dopant or host ions (as discussed in detail in Ref. 4). In light of these observations, it is not so surprising that ScSZ is one of the best zirconia-based ionic conductors (in fact superior to YSZ on that fact alone). It is worth mentioning that this absence of strong vacancy-Sc ordering is in excellent agreement with our previous findings at lower molar concentrations.<sup>4</sup> A second noteworthy finding is that the best way to achieve this nonpreference is to have just enough strain (cation mismatch) so as to cancel out the electronic component (in essence the electrostatic interaction; see below), rather than striving for zero induced strain. The dopant should thus be slightly *larger* than the  $Zr^{4+}$  ion because the elastic interaction reverses sign for dopants smaller than the host ion.

### C. Dopant-dopant interactions

Of the three forms of lattice interactions introduced in Sec. III, the defect ordering tendencies on the cation sublattice of stabilized zirconia are by far the least known about. The nature (i.e., ordering versus clustering tendencies) and the strength of the dopant-dopant interactions and their relative magnitude compared to anion-anion and anion-cation interactions remain wide open questions.

Our analyses of the  $Zr_{10}M_4O_{26}$  compounds are most well suited for extracting interactions on the cation sublattice. In order to understand the choice of compounds considered, we first explain how the stoichiometry, cation, and anion configurations were obtained before proceeding to discuss our results. The 17 mol%  $Zr_{10}M_4O_{26}$  stoichiometry was motivated by reports from Thornber *et al.* on the existence of an ordered  $\gamma$ - $Zr_5Sc_2O_{13}$  phase.<sup>35</sup> This report contains the space group ( $R\bar{3}$ ) and lattice parameters for the  $\gamma$  phase, as well as oxygen and cation sites within the structure.<sup>35</sup> However, no cation ordering was discerned, and thus the Zr/Sc positions in the  $\gamma$  phase are simply given generically as metal ion sites. We have performed a lattice algebra analysis (see Sec. III) to generate all possible cation+anion configurations that are consistent with these observations. This procedure is analogous to the one that we used previously to deduce the lowest-energy configuration of the  $\delta$ - $Zr_3Y_4O_{12}$  phase.<sup>4</sup> The reported crystal structure contains 14 cation positions.<sup>35</sup> An enumeration of all possible 14-cation fluorite-based cells yields a total of 14 402 cation configurations. Of these, only 991 have the proper cation stoichiometry ( $A_4B_{10}$ ), and among these, only 12 have rhombohedral cell vectors. Within this rhombohedral cell, there are four symmetrically distinct cation positions (entirely consistent with the results of Thornber *et al.*) and six distinct anion positions. Since Thornber and co-workers find only five anion positions in the  $\gamma$ - $Zr_5Sc_2O_{13}$  phase,<sup>35</sup> we conclude that both oxygen vacancies in our cell must come from a single anion symmetry type. Only two of our anion positions have a Wyckoff degeneracy of 2, and thus there are only two possible arrangements for the vacancies. Both of these arrangements place vacancies in 3NN positions, i.e., surrounding a single cation, and

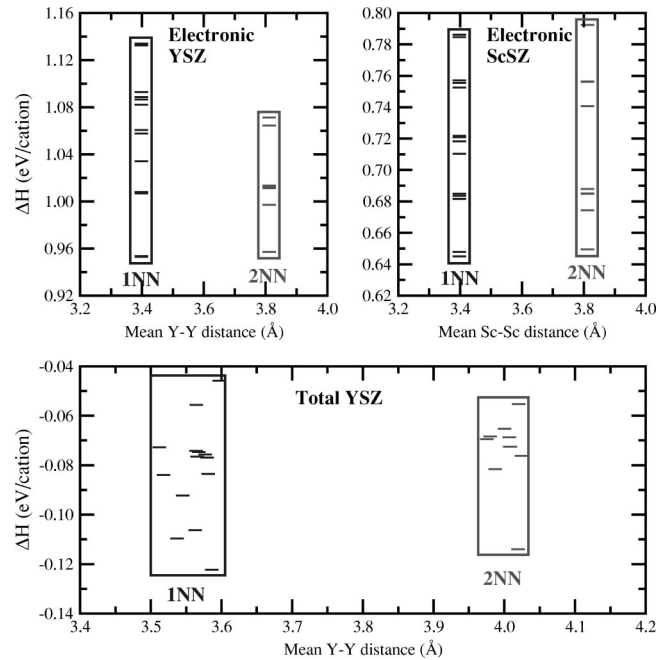


FIG. 8. Calculated formation enthalpies (eV/cation) vs mean dopant-dopant separation for  $Zr_{10}Y_4O_{26}$  (top left and bottom panel) and  $Zr_{10}Sc_4O_{26}$  (top right). The top panels illustrate dopant-dopant defect ordering tendencies in YSZ and ScSZ when elastic interactions are frozen; the bottom panel yields the same information for YSZ when all interactions are taken into account.

thus they both lead to a single sixfold cation position, as observed by Thornber *et al.*<sup>35</sup> (The 3NN vacancy ordering is also precisely what we would expect from our previous findings—see Sec. IV A.) Therefore, the total number of  $Zr_{10}M_4O_{26}$  configurations considered here is 12 (cation configurations)  $\times$  2 (vacancy arrangements) = 24.

Because all of our configurations contain 3NN vacancies, each with distinct possibilities for arranging the cations, we have a structure in which the vacancy-vacancy ordering is fixed, and we can probe the cation-cation (coupled together with cation-anion) interactions. Just as in Sec. IV A, we can then try to extract the dopant-dopant interactions by sorting the data according to the mean dopant-dopant separation.

Figure 8 shows the calculated formation enthalpies (eV/cation) versus average dopant-dopant separation for  $Zr_{10}Y_4O_{26}$  and  $Zr_{10}Sc_4O_{26}$ . In the absence of elastic interactions, electrostatics should prevail, and one would then expect a repulsion between the dopants. A glance at the top panels of Fig. 8 reveals no such trend, however. It seems clear that even in the absence of strain interactions, the vacancy-dopant interactions are sufficiently strong to wash out any trends in dopant-dopant interactions. A corresponding analysis with elastic interactions taken into account (bottom panel of Fig. 8) reveals nothing apparent beyond that.

A different attempt at extracting dopant-dopant interactions can be realized by replotting the data of Fig. 8 with the mean vacancy-dopant separation on the abscissa. Since there are only two average dopant-dopant separations prior to relaxation (about 3.4 and 3.8 Å), we can then see if these structures naturally fall into two groups. Figure 9 shows

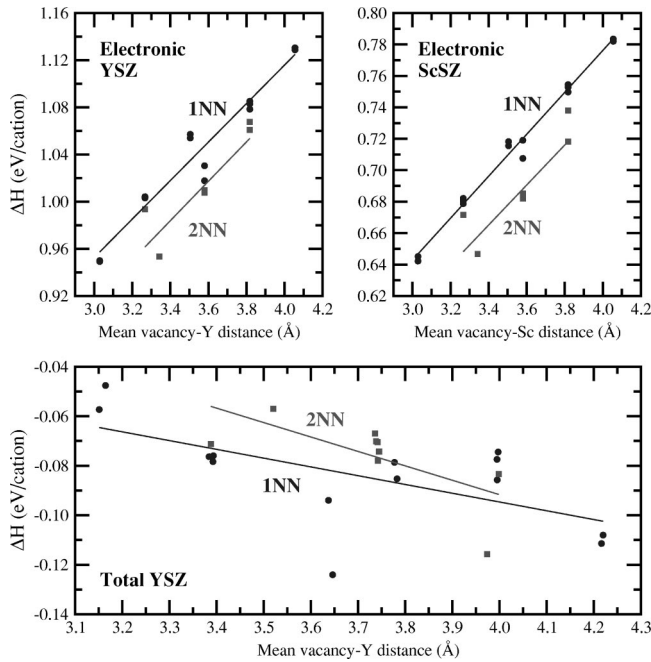


FIG. 9. The same data as in Fig. 8, this time redrawn with the mean vacancy-dopant separation on the horizontal axis.

these results, where this time the degree of shading (filled/shaded) represents the mean dopant-dopant separation. In the case of relaxed structures, we simply adopt the grouping symbol of the unrelaxed structure.

This way of sorting the data turns out to be more helpful. We first focus on the top panels of Fig. 9, where elastic interactions are frozen. At any given vacancy-dopant separation, NN dopant compounds in both YSZ and ScSZ always have a higher formation enthalpy than the 2NN dopant compounds. This observed dopant-dopant repulsion is exactly what one would expect to find from simple electrostatic considerations. Thus, just as in the vacancy-vacancy and vacancy-dopant ordering cases, the electrostatically expected defect ordering is observed when relaxations are frozen. We note that the positive slopes in all unrelaxed calculations are in excellent agreement with our previous findings in Sec. IV B for other structures at different compositions.

Once we do allow relaxations, the results for YSZ (bottom panel) show that NN dopants become slightly favorable and that there hence seems to be a slight dopant-dopant attraction. The energy scale here is substantially smaller than for vacancy-vacancy and even vacancy-dopant ordering, indicating again that dopant-dopant interactions are the weakest ones in the system. Thus, as in all previous cases, the elastic dopant-dopant interactions counteract the electrostatically preferred defect ordering at all probed defect separations.

It is also interesting to note the considerably smaller negative slopes in the bottom panel of Fig. 9 compared with those in Fig. 6. This suggests a palpably weaker vacancy-dopant ordering preference at the considerably larger vacancy-dopant separations in  $Zr_{10}Y_4O_{26}$  compared with  $Zr_3Y_4O_{12}$  (see discussion in Sec. IV B), as expected given the established nature of the defect interactions.

## V. ROLE OF ELECTROSTATICS

Throughout the paper, we have often used the term electronic interaction, and yet we have looked at electrostatics for guidance about defect ordering. The “electronic” part encompasses the full classical and quantum-mechanical electronic interactions, including multipole interactions, ionic polarization, etc., as calculated within density-functional theory. The objective of the following analysis is to assess the fraction of the electronic term that is comprised of simple classical point-charge electrostatics. There are several reasons for doing this analysis. For one, it is considerably easier to comprehend and extrapolate results from classical electrostatics than from a full quantum-mechanical description. Second—and just as importantly—we can assess the extent of variation in defect ordering that is attainable through variations in the electronic properties of the constituent ions. In other words, it would be interesting to assess the extent to which defect ordering could be controlled via variations in (beyond point-charge electrostatics) electronic properties.

To perform this analysis, we separately compute the electrostatic energy of an array of point charges situated in the 45 possible anion-cation arrangements of the  $\delta$  structure using a standard Ewald summation technique. We then compare the energies of these calculations with those of our electronic structure calculations. Throughout the electrostatical calculations, ideal point charges are used (4+ for host and 3+ for dopant cations, 2− for oxygen anions).

Figure 10 illustrates these results as compared with the full DFT calculations for the same set of structures (with the strain term frozen). The upper panel in Fig. 10 shows the DFT calculations (which are identical to the middle panel of Fig. 6), while the lower panel shows the point-charge electrostatic energy. Clearly, the results look quite similar. In particular, identical trends are found for vacancy-vacancy ordering (3NN preferred) and vacancy-dopant ordering (vacancy-Y association preferred). The inset in the lower panel shows a plot of the DFT results versus the electrostatics calculations. The fact that all 45 data points fall very close to a straight line shows that the electronic (unrelaxed) part of the YSZ (and ScSZ) calculations is almost purely due to electrostatics. Thus, speciation of defect ordering for a given class of aliovalent dopants is left almost entirely to the elastic term, which is strongly coupled to the size of the dopants. In a recent report, we demonstrate the coupling between defect ordering and ionic conduction by screening a number of divalent and trivalent dopants set apart primarily by their ionic radius.<sup>4</sup>

The fact that the electronic part of the defect interactions is almost entirely due to point-charge electrostatics bears some additional consequences. For one, we would not expect appreciable changes in defect ordering or ionic conductivity solely due to variations in electronic parameters like polarizability, electronegativity, etc. Yet this is seemingly what has recently been reported for rare-earth-doped cubic bismuth oxides, namely, that ionic conductivity and its decay time scale linearly with dopant polarizability.<sup>37</sup> The apparent resolution to this conflict is that the classical dopant polarizability is proportional to the cube of the ionic radius. (This rela-

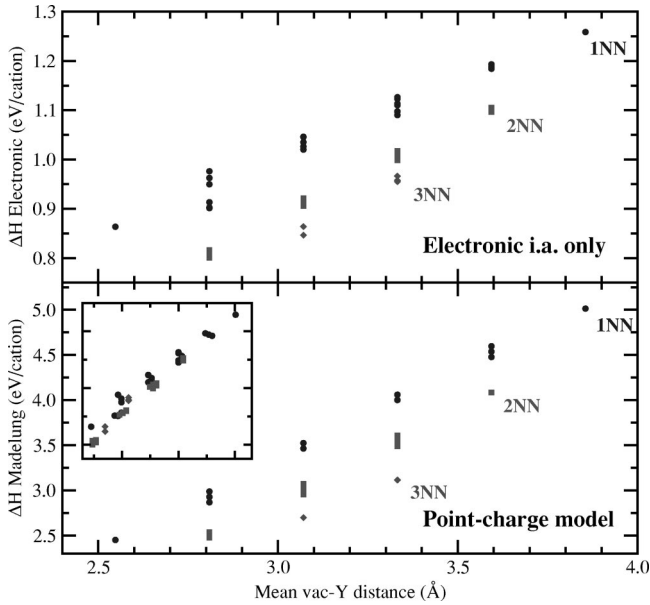


FIG. 10. Comparison between full electronic structure DFT calculations with strain frozen out (top panel) and classical electrostatic field summation of the 45 isomorphs for the formation enthalpies of the  $\delta$  compound  $Zr_3Y_4O_{12}$  (bottom panel). The circles, squares, and diamonds represent 1NN, 2NN, and 3NN vacancy-vacancy configurations, respectively. The inset in the lower panel compares the formation enthalpies against each other; the small deviations from a straight line shows the dominating effect of electrostatics in the total electronic part of the defect interactions.

tion is, in fact, how the polarizability is computed in the experimental study.<sup>37)</sup> Thus, according to our analyses, the experimentally measured correlation between ionic conduction decay times and polarizability is due to the fact that the polarizability increases rapidly with ion size, *not* due to the polarization itself. In other words, if it were possible to affect the polarizability without changing the ionic radius, we would expect this correlation to vanish.

## VI. ORDERED GROUND STATES

Ordered compounds in any phase diagram are of considerable interest for various reasons. In electrolyte applications, one tries to avoid ordered compounds since they are believed to significantly reduce ion mobility by trapping carriers in low-energy states. Although it is possible to avoid the formation of ordered phases, short-range signatures of long-range ordered compounds can often survive in solid solutions “far” away from the actual ordered phase in both composition and temperature. Thus, it is exceedingly important to understand the stability and type of ordered compounds for optimizing a material’s properties.

Given the calculated energy-composition relations, depicted in Figs. 2 and 3, we can begin to address the question of what the stable (low-temperature) “ground states” in the YSZ and ScSZ systems are. The necessary criterion for a ground-state compound is that the ground state must be lower in energy than any other structure at the particular

composition, as well as any two-phase mixture of structures at other compositions. Following this criterion, energies at the  $T=0$  ground states of a system must lie on a so-called convex hull where tie lines are drawn between low-energy phases, with only the minimum-energy lines retained. These segments must necessarily be convex upward, since any concave downward region would indicate an instability towards phase separation between two neighboring phases.

Although we have a seemingly large number (nearly 300) of configurations sampled for the YSZ and ScSZ systems, this number still pales in comparison to the astronomically large number of configurational possibilities allowed ( $2^N$  for  $N$  ionic positions). All of our convex hull constructions in Figs. 2 and 3 should therefore be seen as upper bounds to the true ground-state hull. It is quite possible that unexpected low-energy structures could still exist beyond the 300 that we have explored. However, for the stoichiometries where compounds have been experimentally reported ( $Zr_3M_4O_{12}$  and  $Zr_5M_2O_{13}$ ), we have (as explained above) considered all possible configurations consistent with experimental observations. We therefore expect that the lowest-energy structures *at these compositions* are the true ground-state configurations on the convex hull, as remains to be verified experimentally.

Based on such an analysis, we recently reported the discovery of new metastable zirconia-rich compounds in the YSZ phase diagram.<sup>4</sup> We also completed the experimentally known information about the  $\delta$ - $Zr_3Y_4O_{12}$  compound by establishing its full crystal structure. In the following, we present a similar analysis for the ScSZ system and make detailed comparisons with YSZ results.

We have drawn two different convex hull constructions in Figs. 2 and 3: one considering only the cubic fluorite-based configurations (solid lines) and one considering all structures, i.e., including the monoclinic and tetragonal phases of  $ZrO_2$  (dashed lines). We distinguish between these two constructions because the first-principles energy differences between three forms of  $ZrO_2$  have been shown to be either smaller (LDA) or larger (GGA) than those deduced from experiment (see Ref. 4 and references therein). In all cases, the “cubic-only” convex hulls are consistent with experimental phase diagrams, whereas some discrepancies arise for the “full” convex hulls. These discrepancies seem to suggest the possibility that the error lies in the first-principles energies of the monoclinic and tetragonal  $ZrO_2$  phases, rather than any errors in the cubic ordered phases. For the YSZ system, the “cubic-only” convex hull contains four phases  $ZrO_2$ ,  $Y_2O_3$ ,  $\delta$ - $Zr_3Y_4O_{12}$ , and the previously predicted Zr-rich compound  $Zr_6Y_2O_{15}$ . This last structure is particularly interesting, because the tie line between this and the  $\delta$  phase lies lower in energy than any of the  $Zr_5M_2O_{13}$  structures (observed in ScSZ but not YSZ). The “full” convex hull in YSZ contains only  $ZrO_2$  (monoclinic),  $Y_2O_3$ , and  $\delta$ - $Zr_3Y_4O_{12}$ , which are in fact the only three phases observed at low temperatures in YSZ. On the other hand, the ScSZ ground-state diagrams are quite different from those of YSZ. For the “cubic-only” convex hull, we again have four phases  $ZrO_2$ ,  $Sc_2O_3$ ,  $\delta$ - $Zr_3Sc_4O_{12}$ , but for ScSZ the observed  $\gamma$ - $Zr_5Sc_2O_{13}$  phase is also on the hull. However, the

TABLE I. Ionic coordinates for the  $\delta$ -Zr<sub>3</sub>Sc<sub>4</sub>O<sub>12</sub> structure, as computed within the DFT-GGA. The fully relaxed cation and anion coordinates, as well as the ideal anion vacancy positions  $s_1$ – $s_3$ , are given in scaled (direct) space, with the matrix multiplier (unit cell vectors) for conversion to Cartesian coordinates provided in the first three lines ( $\mathbf{a}_1$ – $\mathbf{a}_3$ ), in units of Å. The last column shows the coordination number  $n$  for cations, anions, and anion vacancies.

Unit cell vectors				
$\mathbf{a}_1$	5.0964	2.5474	2.5494	
$\mathbf{a}_2$	-2.5491	5.0978	2.5477	
$\mathbf{a}_3$	-2.5483	-2.5476	5.0961	
Ion	$s_1$	$s_2$	$s_3$	$n$
Zr	0.3875	0.1394	0.7003	O <sub>7</sub>
	0.8605	0.2998	0.3876	O <sub>7</sub>
	0.7002	0.6125	0.8606	O <sub>7</sub>
Sc <sub>1</sub>	0.0087	0.9914	0.0086	O <sub>6</sub>
Sc <sub>2</sub>	0.3108	0.3955	0.1349	O <sub>7</sub>
	0.1352	0.6890	0.6044	O <sub>7</sub>
	0.6045	0.8649	0.3107	O <sub>7</sub>
O <sub>1</sub>	0.3286	0.0682	0.0738	Zr <sub>1</sub> Sc <sub>3</sub>
	0.0737	0.6714	0.9317	
	0.9319	0.9261	0.3287	
O <sub>2</sub>	0.6822	0.9383	0.9093	Zr <sub>2</sub> Sc <sub>2</sub>
	0.0616	0.0912	0.6823	
	0.9091	0.3178	0.0618	
O <sub>3</sub>	0.1771	0.4189	0.4228	Zr <sub>2</sub> Sc <sub>2</sub>
	0.5810	0.5772	0.1770	
	0.4228	0.8229	0.5811	
O <sub>4</sub>	0.5737	0.1815	0.4324	Zr <sub>2</sub> Sc <sub>2</sub>
	0.4325	0.4263	0.8184	
	0.8183	0.5676	0.5735	
$\square_1$	0.7500	0.2500	0.7500	Zr <sub>2</sub> Sc <sub>2</sub>
$\square_2$	0.2500	0.7500	0.2500	Zr <sub>1</sub> Sc <sub>3</sub>

“full” convex hull contains only the ZrO<sub>2</sub>(monoclinic) and Sc<sub>2</sub>O<sub>3</sub> phases; even the  $\delta$ -Zr<sub>3</sub>Sc<sub>4</sub>O<sub>12</sub> lies above this tie line. This latter point is in seeming contrast to experimental observations of low-temperature phases in this system. As mentioned above, a plausible cause of this discrepancy is in the first-principles energy for the monoclinic phase.

Another point of interest is to compare the crystal structures of the  $\delta$  compound, which forms ordered phases in both YSZ and ScSZ. The structure of Zr<sub>3</sub>Y<sub>4</sub>O<sub>12</sub> is relatively easy to understand in terms of the strong preference for  $\langle 111 \rangle$  vacancy ordering and vacancy-Zr association in YSZ. Since we find the same vacancy ordering preference in ScSZ (see Sec. IV A), there is obviously a great similarity between the two  $\delta$  compounds. However, given the weaker elastic component of vacancy-dopant interactions in ScSZ than YSZ and the concomitant weak preference for any particular vacancy-dopant ordering, there is little reason to expect the two ordered phases to be identical. Consequently, there is little surprise in noting that the lowest-energy structure of  $\delta$ -Zr<sub>3</sub>Sc<sub>4</sub>O<sub>12</sub> has a different cation arrangement than

TABLE II. Ionic coordinates for the  $\gamma$ -Zr<sub>10</sub>Sc<sub>4</sub>O<sub>26</sub> structure, as computed within the DFT-GGA. See Table I for an explanation of the nomenclature.

Unit cell vectors					
$\mathbf{a}_1$	7.7463	2.5411	-0.0477		
$\mathbf{a}_2$	-0.0484	7.7214	2.5439		
$\mathbf{a}_3$	2.5495	-0.0450	7.7181		
Ion	$s_1$	$s_2$	$s_3$	$n$	
Zr	0.0412	0.6359	0.7875	O <sub>8</sub>	
	0.4047	0.9006	0.7091	O <sub>7</sub>	
	0.7544	0.1035	0.6577	O <sub>8</sub>	
	0.4937	0.5029	0.4994	O <sub>6</sub>	
	0.8987	0.7115	0.4095	O <sub>7</sub>	
	0.2099	0.9551	0.3671	O <sub>8</sub>	
	0.5956	0.1009	0.2843	O <sub>7</sub>	
	0.9497	0.3636	0.2154	O <sub>8</sub>	
	0.2905	0.5903	0.0993	O <sub>7</sub>	
	0.6369	0.7887	0.0438	O <sub>8</sub>	
	Sc	0.0116	0.0127	0.0050	O <sub>8</sub>
		0.3565	0.2143	0.9493	O <sub>8</sub>
0.7104		0.4042	0.8989	O <sub>7</sub>	
0.1049		0.2924	0.5969	O <sub>7</sub>	
O		0.1374	0.1365	0.1406	Zr <sub>2</sub> Sc <sub>2</sub>
		0.8481	0.8640	0.8384	Zr <sub>3</sub> Sc <sub>1</sub>
	0.4721	0.3258	0.0969	Zr <sub>2</sub> Sc <sub>2</sub>	
	0.2199	0.1142	0.8092	Zr <sub>1</sub> Sc <sub>3</sub>	
	0.8309	0.5478	0.0125	Zr <sub>3</sub> Sc <sub>1</sub>	
	0.5740	0.3407	0.7436	Zr <sub>2</sub> Sc <sub>2</sub>	
	0.1863	0.7826	0.8798	Zr <sub>3</sub> Sc <sub>1</sub>	
	0.8963	0.5291	0.6717	Zr <sub>2</sub> Sc <sub>2</sub>	
	0.5353	0.0042	0.8426	Zr <sub>3</sub> Sc <sub>1</sub>	
	0.3866	0.7585	0.5397	Zr <sub>4</sub> Sc <sub>0</sub>	
	0.8899	0.1881	0.7933	Zr <sub>1</sub> Sc <sub>3</sub>	
	0.6767	0.9067	0.5232	Zr <sub>4</sub> Sc <sub>0</sub>	
	0.2462	0.4546	0.6366	Zr <sub>2</sub> Sc <sub>2</sub>	
	0.9834	0.1639	0.4588	Zr <sub>3</sub> Sc <sub>1</sub>	
	0.0365	0.8089	0.5378	Zr <sub>4</sub> Sc <sub>0</sub>	
	0.7593	0.5416	0.3785	Zr <sub>4</sub> Sc <sub>0</sub>	
	0.3273	0.1018	0.4723	Zr <sub>3</sub> Sc <sub>1</sub>	
	0.1205	0.8094	0.2124	Zr <sub>3</sub> Sc <sub>1</sub>	
0.6149	0.2492	0.4489	Zr <sub>4</sub> Sc <sub>0</sub>		
0.4549	0.9809	0.1752	Zr <sub>3</sub> Sc <sub>1</sub>		
0.1027	0.4742	0.3275	Zr <sub>3</sub> Sc <sub>1</sub>		
0.8110	0.2171	0.1249	Zr <sub>2</sub> Sc <sub>2</sub>		
0.4591	0.6176	0.2407	Zr <sub>4</sub> Sc <sub>0</sub>		
0.1620	0.4533	0.9952	Zr <sub>3</sub> Sc <sub>1</sub>		
0.7876	0.8818	0.1811	Zr <sub>3</sub> Sc <sub>1</sub>		
0.5224	0.6706	0.8952	Zr <sub>3</sub> Sc <sub>1</sub>		
$\square_1$	0.6250	0.6250	0.6250	Zr <sub>3</sub> Sc <sub>1</sub>	
$\square_2$	0.3750	0.3750	0.3750	Zr <sub>3</sub> Sc <sub>1</sub>	

$\delta$ -Zr<sub>3</sub>Y<sub>4</sub>O<sub>12</sub>. While in the YSZ  $\delta$  phase it is a Zr (host) ion which assumes the only sixfold-coordinated position right in between the two third-neighboring vacancies, in the ScSZ  $\delta$  phase that position is occupied by a Sc (dopant) ion. The energetic penalty associated with changing the preferred structure of the respective  $\delta$  phases to that of its counterpart is 21 meV/cation for  $\delta$ -ScSZ in the  $\delta$ -YSZ structure and 91 meV/cation for the opposite scenario. This smaller energetic penalty for cation “antisites” is consistent with the observations of complete lack of cation order in  $\delta$ -Zr<sub>3</sub>Sc<sub>4</sub>O<sub>12</sub> (Refs. 35 and 36) and, in contrast, distinct cation order in Zr<sub>3</sub>Y<sub>4</sub>O<sub>12</sub> (and Zr<sub>3</sub>Yb<sub>4</sub>O<sub>12</sub>) (Ref. 36).

## VII. SUMMARY

We have performed a detailed analysis of defect ordering in yttria- and scandia-doped cubic zirconia at a wide range of dopant concentrations using first-principles calculations. The specific elucidation of the origins of the reported defect ordering preferences provides a coherent and robust means of understanding the defect chemistry in a wide class of doped (zirconium) oxides and can be used as effective guidance in efforts to optimize materials properties like ionic conductivity and electrolyte heat treatments. Specifically, our results show that defect ordering in stabilized zirconia is most strongly governed by vacancy-vacancy interactions, followed by vacancy-dopant and, weakest of all, dopant-dopant interactions. We show that all observed ordering tendencies can be well understood in terms of a balance between competing electrostatic and elastic defect interactions, the latter of which account for dopant speciation. In particular, we show that the best way to minimize the vacancy-dopant association deleterious to ionic conduction is to choose dopants whose strain term maximally counteracts the electrostatic interaction term, rather than striving for zero induced strain. This result is well exemplified by our finding that there is a negligible vacancy-dopant association in ScSZ, while in YSZ the larger strain component due to the larger ionic radius of yttrium ions leads to a strong vacancy-Zr association that hampers ionic conduction by vacancy diffusion.

## APPENDIX

In this appendix, we report the full crystal structures of the  $\delta$  and  $\gamma$  phases of ScSZ, to complement our previous report for the  $\delta$  phase of YSZ (Ref. 4) and compare their defect structures.

Table I contains a complete set of coordinates for the  $\delta$ -Zr<sub>3</sub>Sc<sub>4</sub>O<sub>12</sub> structure, as computed within the DFT-GGA. In comparing with the  $\delta$ -Zr<sub>3</sub>Y<sub>4</sub>O<sub>12</sub> structure, previously reported in Ref. 4, we note some distinct differences. First of all, the  $\delta$  compound in ScSZ has a different cation structure (*B*) than that in YSZ (*A*) to use our previous terminology. Further, in YSZ, the two vacancies in the lattice are symmetrically equivalent, while in ScSZ that is not the case. Taking into account these different symmetry lowering distinctions, we note that there are only four symmetrically distinct oxygen positions in  $\delta$ -ScSZ, as compared to six in  $\delta$ -YSZ. Moreover, all Zr ions are equivalent in the former case, unlike in YSZ. From a physical point of view, the main difference is that in  $\delta$ -ScSZ the only sixfold-coordinated cation is a dopant ion (Sc), while in  $\delta$ -YSZ it is a host ion (Zr) that occupies this position. As discussed in previous sections, the latter observation is consistent with the large driving force for  $\square$ -Zr association in YSZ. In ScSZ, there is no clear vacancy-cation preference (see, e.g., Fig. 7) and thus no reason to expect any particular cation to assume the sixfold coordination. As it turns out, it is a dopant ion that ends up occupying the least coordinated crystal position.

In Table II, we specify the ionic coordinates for the  $\gamma$ -ScSZ structure Zr<sub>10</sub>Sc<sub>4</sub>O<sub>26</sub>. Upon relaxing the ideal crystal positions of the 24 candidate structures (see Sec. IV A 2), we noted somewhat larger ionic relaxations than in any of the other structures considered in this study. In the most severe case we noted a cation relaxation of about 0.26 Å and an anion relaxation of about 0.79 Å, and the structure thereby basically collapsed into that of another starting structure. Given the different relaxation patterns of these two structures, the resulting coordinates were found to differ slightly. The largest noted uncertainty was about 0.11 Å for an oxygen ion position, indicating the accuracy of stated ionic coordinates in Table II. The energies of the two structures were identical to within  $3 \times 10^{-5}$  eV, indicating cumulative small differences in ionic positions.

<sup>1</sup>V. V. Kharton, E. N. Naumovich, and A. A. Vecher, *J. Solid State Electrochem.* **3**, 61 (1999); V. V. Kharton, A. A. Yaremchenko, and E. N. Naumovich, *ibid.* **3**, 303 (1999).

<sup>2</sup>T. H. Etsell and S. N. Flengas, *Chem. Rev.* **70**, 339 (1970).

<sup>3</sup>J. Kondoh, T. Kawashima, S. Kikuchi, Y. Tomii, and Y. Ito, *J. Electrochem. Soc.* **145**, 1527 (1998); J. Kondoh, S. Kikuchi, Y. Tomii, and Y. Ito, *Physica B* **262**, 177 (1999).

<sup>4</sup>A. Bogicevic, C. Wolverton, G. M. Crosbie, and E. B. Stechel, *Phys. Rev. B* **64**, 014106 (2001).

<sup>5</sup>A. Bogicevic and C. Wolverton, *Europhys. Lett.* **56**, 393 (2001).

<sup>6</sup>D. Steele and B. E. F. Fender, *J. Phys. C* **7**, 1 (1974).

<sup>7</sup>W. L. Roth, R. Wong, A. I. Goldman, E. Canova, Y. H. Kao, and

B. Dunn, *Solid State Ionics* **18-19**, 1115 (1986).

<sup>8</sup>M. H. Tuilier, J. Dexpert-Ghys, H. Dexpert, and P. Lagarde, *J. Solid State Chem.* **69**, 153 (1987).

<sup>9</sup>H. Morikawa, Y. Shimizugawa, F. Marumo, T. Harasawa, H. Ikawa, K. Tohji, and Y. Udagawa, *J. Ceram. Soc. Jpn.* **96**, 253 (1988).

<sup>10</sup>Z. J. Shen, T. K. Li, K. Q. Lu, and Y. Q. Zhao, *Guisuanyan Xuebao* **16**, 270 (1988).

<sup>11</sup>X. Li and B. Hafskjold, *J. Phys.: Condens. Matter* **7**, 1255 (1995).

<sup>12</sup>C. R. A. Catlow, A. V. Chadwick, G. N. Greaves, and L. M. Moroney, *J. Am. Ceram. Soc.* **69**, 272 (1986).

<sup>13</sup>M. Cole, C. R. A. Catlow, and J. P. Dragan, *J. Phys. Chem. Solids*

- 51**, 507 (1990).
- <sup>14</sup>F. Shimojo, T. Okabe, F. Tachibana, M. Kobayashi, and H. Okazaki, *J. Phys. Soc. Jpn.* **61**, 2848 (1992).
- <sup>15</sup>P. Li, I-W. Chen, and J. E. Penner-Hahn, *Phys. Rev. B* **48**, 10 074 (1993); *J. Am. Ceram. Soc.* **77**, 118 (1994).
- <sup>16</sup>J. P. Goff, W. Hayes, S. Hull, M. T. Hutchings, and K. N. Clausen, *Phys. Rev. B* **59**, 14 202 (1999).
- <sup>17</sup>S. Gennard, F. Corà, and C. R. A. Catlow, *J. Phys. Chem. B* **103**, 10 158 (1999).
- <sup>18</sup>G. Stapper, M. Bernasconi, N. Nicoloso, and M. Parrinello, *Phys. Rev. B* **59**, 797 (2000).
- <sup>19</sup>S. Ostanin, A. J. Craven, D. W. McComb, D. Vlachos, A. Alavi, A. T. Paxton, and M. W. Finnis, *Phys. Rev. B* **65**, 224109 (2002).
- <sup>20</sup>Within a given class of aliovalent dopants.
- <sup>21</sup>P. Hohenberg and W. Kohn, *Phys. Rev.* **136**, B864 (1964).
- <sup>22</sup>W. Kohn and L. J. Sham, *Phys. Rev.* **140**, A1133 (1965).
- <sup>23</sup>D. Vanderbilt, *Phys. Rev. B* **32**, 8412 (1985).
- <sup>24</sup>G. Kresse and J. Hafner, *Phys. Rev. B* **47**, 558 (1993); **49**, 14 251 (1994); G. Kresse and J. Furthmuller, *ibid.* **54**, 11 169 (1996).
- <sup>25</sup>J. P. Perdew, in *Electronic Structure of Solids 1991*, edited by P. Ziesche and H. Eschrig (Akademie-Verlag, Berlin, 1991), Vol. 11.
- <sup>26</sup>D. M. Ceperley and B. J. Alder, *Phys. Rev. Lett.* **45**, 566 (1980);
- J. P. Perdew and A. Zunger, *Phys. Rev. B* **23**, 5048 (1981).
- <sup>27</sup>L. G. Ferreira, S.-H. Wei, and A. Zunger, *Int. J. Supercomput. Appl.* **5**, 34 (1991).
- <sup>28</sup>Bixbyite is the equilibrium phase for  $Y_2O_3$  and  $Sc_2O_3$ . We have also looked in detail at about 20 other higher-energy  $Y_2O_3$  structures, the results of which are not reported in this study.
- <sup>29</sup>Throughout the paper we maintain the enthalpy notation  $\Delta H$  also for constant-volume calculations where we are isolating electronic interactions, although strictly speaking these are formation energies and not enthalpies.
- <sup>30</sup>H. G. Scott, *Acta Crystallogr., Sect. B: Struct. Crystallogr. Cryst. Chem.* **33**, 281 (1977).
- <sup>31</sup>V. S. Stubican, J. R. Hellmann, and S. P. Ray, *Mater. Sci. Monogr.* **10**, 257 (1982).
- <sup>32</sup>S. P. Ray, V. S. Stubican, and D. E. Cox, *Mater. Res. Bull.* **15**, 1419 (1980).
- <sup>33</sup>M. Sakib Khan, M. Saiful Islam, and D. R. Bates, *J. Mater. Chem.* **8**, 2299 (1998).
- <sup>34</sup>M. O. Zacate, L. Minervini, D. J. Bradfield, R. W. Grimes, and K. E. Sickafus, *Solid State Ionics* **128**, 243 (2000).
- <sup>35</sup>M. R. Thornber, D. J. M. Bevan, and J. Graham, *Acta Crystallogr., Sect. B: Struct. Crystallogr. Cryst. Chem.* **24**, 1183 (1968).
- <sup>36</sup>H. J. Rossell, *J. Solid State Chem.* **19**, 103 (1976).
- <sup>37</sup>E. D. Wachsman, S. Boyapati, and N. Jiang, *Ionics* **7**, 1 (2001).